Soft Matter

Accepted Manuscript

ROYAL SOCIETY OF CHEMISTRY

www.rsc.org/softmatter

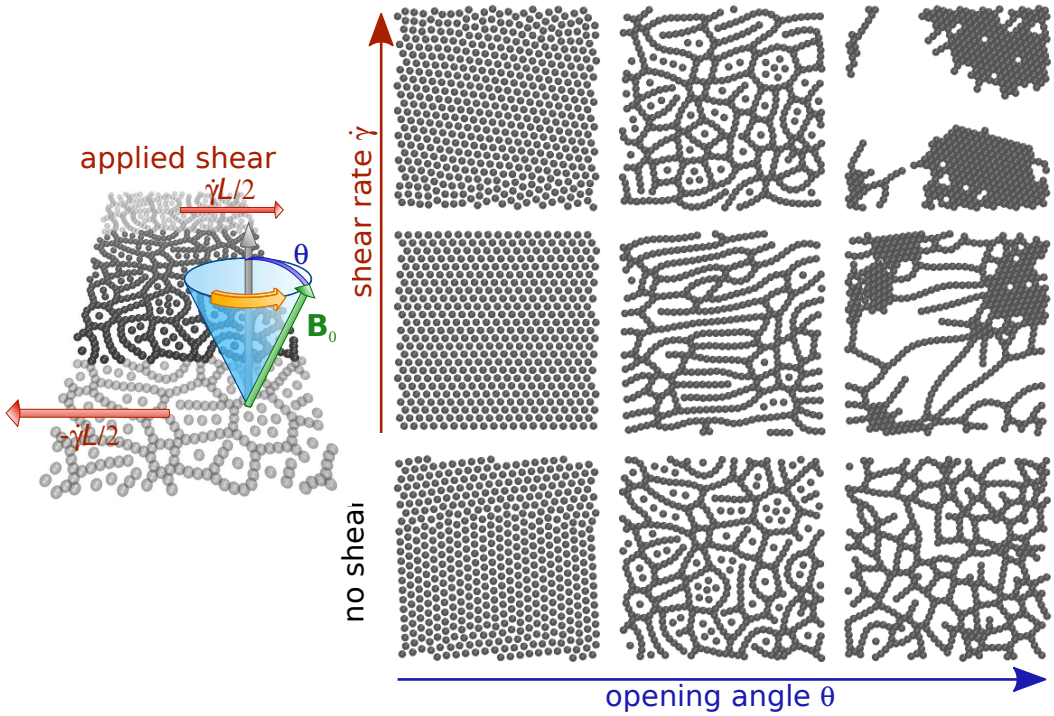

FIG. 1. We explore the response of 2D magnetic colloids in precessing external field to a steady shear and find three major mechanisms of stress release.

Two-dimensional magnetic colloids under shear

Tomaž Mohorič,[1,2] Jure Dobnikar*,[1] and Jürgen Horbach[3]

[1] *International Research Centre for Soft Matter, Beijing University of Chemical Technology, Beijing 100029, P.R. China*
[2] *Faculty of Chemistry and Chemical Technology, University of Ljubljana, Večna pot 113, 1000 Ljubljana, Slovenia*
[3] *Institute for Theoretical Physics II: Soft Matter, Heinrich-Heine-Universität Düsseldorf, 40225 Düsseldorf, Germany*

Complex rheological properties of soft disordered solids, such as colloidal gels or glasses, inspire a range of novel applications. However, the microscopic mechanisms of their response to mechanical loading are not well understood. Here, we elucidate some aspects of these mechanisms by studying a versatile model system, i.e. two-dimensional superparamagnetic colloids in a precessing magnetic field, whose structure can be tuned from a hexagonal crystal to a disordered gel network by varying the external field opening angle θ. We perform Langevin dynamics simulations subjecting these structures to a constant shear rate and observe three qualitatively different types of material response. In hexagonal crystals ($\theta = 0°$), at sufficiently low shear rate, plastic flow occurs via successive stress drops at which the stress releases due to the formation of dislocation defects. The gel network at $\theta = 48°$, on the contrary, yields via bond rearrangement and transient shear banding evolving into a homogeneously stretched network at large strains. The latter structure remains metastable after switching off of the shear. At $\theta = 50°$, the external shear makes the system unstable against phase separation and causes a failure of the network structure leading to the formation of hexagonal close packed clusters interconnected by particle chains. On a microcopic level, our simulations provide insight into some of the mechanisms mechanisms by which strain localization as well as material failure occur in a simple gel-like network. Furthermore, we demonstrate that new stretched network structures can be generated by the application of shear.

I. INTRODUCTION

Understanding the response of amorphous solids to mechanical loading is a major issue in materials science and technology [1, 2]. Recently, amorphous solids with a dense packing of particles such as metallic or colloidal glasses have been extensively studied in this respect [3–28]. A peculiar feature in these systems is strain localization in form of long-lived shear bands [1, 16–19, 27] that lead to stuctural inhomogeneities with significant density variations in the shear-band regions, even after the mechanical loading is switched off [8, 9, 28]. Similar inhomogeneous flow patterns in solids with a disordered network structure have been much less in the focus of recent research. These systems comprise a wide variety of materials, ranging from colloidal gels [29–33] and (bio-)polymer networks [34–38] to glass-formers with a tetrahedral network structure (e.g. SiO_2 [39, 40]), with a rich variety in their mechanical response including strain localization [39, 41–44], mechanical failure due to crack propagation [45] or an induced phase separation [46, 47], and the formation of deformed network structures that remain metastable when the external load is switched off [48, 49]. Despite the importance of these features in materials science, they are currently not well understood on the microscopic level. To this end, an amorphous network model system, which can be realized experimentally and reveals generic properties of the response to external mechanical fields, would be useful.

Recently, a two-dimensional colloidal system that possibly fulfills these requirements has been presented by Müller *et al.* [50] using a combination of simulation and experiment. The two-dimensional system consists of superparamagnetic colloids, subjected to an external magnetic field that precesses around the axis in the direction perpendicular to the colloidal plane. The opening angle θ of the cone on which the field is precessing, controls the nature of colloidal interactions and the structure formation in the system. At $\theta = 0°$ the repulsive dipolar interactions result in hexagonal crystals, while at $\theta = 90°$ the interaction is purely attractive dipolar, which makes the system unstable against aggregation. Within the range of intermediate θ values, a mixture of short-range attractive and long-range repulsive interactions drive the assembly of gel-like structure, consisting of a network of percolating chains in coexistence with free particles.

Here, we investigate the response of such two-dimensional colloidal systems to external shear using Langevin dynamics computer simulations. A planar Couette flow geometry is considered and the systems are sheared at various constant shear rates. We focus on three opening angles $\theta = 0°$, $\theta = 48°$, and $\theta = 50°$, where we observe three qualitatively different mechanisms of stress release. The schematic illustration of the geometry and the summary of three different respnse mechanisms are presented in Figure 1. At $\theta = 0°$, a transition towards plastic flow occurs, provided that the shear rate is low enough. Similar as in earlier studies [51–55], the flow in the crystal is maintained by dislocation defects, associated with successive stress drops at which the stress is released by the formation and transport of the dislocations. A completely different response to the shear is observed for the amorphous network structures at the other two angles. For $\theta = 48°$, the stress-strain relations show

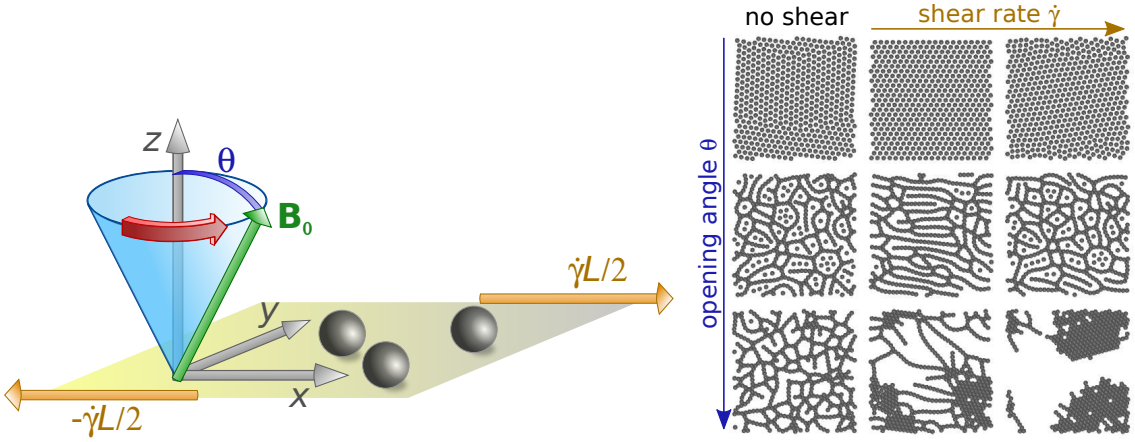

FIG. 1. Schematic illustration of the system (left) and the state diagram (right) epitomizing the observed phenomena.

an overshoot at a strain around $\gamma \approx 1.0$. For $\gamma > 1.0$, transient shear bands emerge that finally evolve into a stretched network structure. This structure remains at least metastable after the switch-off of the shear, indicating that the network can be transformed into a new stretched state by the application of shear. For $\theta = 50°$, the network becomes unstable against phase separation beyond a strain $\gamma \approx 1.0$, corresponding again to the maximum in the stress-strain relation. In this case, clusters with hexagonal crystalline structure are formed that are connected to each other by chains of particles and that might eventually evolve into one large crystalline cluster.

The rest of the paper is organized as follows. In Sec. II, the main details of the simulation are described. In Sec. III we present our results on the three microscopic mechanisms of the response to the external shear followed by a summary and conclusions in Sec. IV.

II. DETAILS OF THE SIMULATION

We performed Langevin dynamics simulations of superparamagnetic colloids under precessing external field $\mathbf{B}_0 = B_0\,(\sin\theta\cos\omega t, \sin\theta\sin\omega t, \cos\theta)$ with magnitude B_0, frequency ω and opening angle θ. Colloids are modelled as soft spheres of diameter σ (via a Weeks-Chandler-Andersen potential [56]) with an induced point-like magnetic moment in the center. On a pair level, the interaction potential $V(r)$ induced by the external field between two colloids separated by distance r ranges from repulsive dipolar interaction ($V(r) \propto r^{-3}$) at $\theta = 0°$ to purely attractive dipolar interaction ($V(r) \propto -r^{-3}$) at $\theta = 90°$. In an intermediate range of the opening angles, $45° \leq \theta \leq 60°$, the external magnetic field induces a mixture of short-range attractive and long-range repulsive interactions, associated with pronounced many-body effects (i.e. the interactions between the particles are not pairwise-additive). At the magic angle, $\theta_m = 54.7°$, the potential becomes attractive with $V(r) \propto -r^{-6}$, i.e. van-der-Waals-like interactions are obtained [57–59]. Here we do not rely on pairwise additivity assumption but calculate the full many-body interaction potential in a dense system. The magnetic dipole $\mathbf{m}_i$ of the i-th particle is proportional to the local magnetic field (i.e. external field plus depolarization contributions of the other dipoles) [50, 58]:

$$\mathbf{m}_i(t) = \frac{4\pi\sigma^3\chi}{24\mu_0}\left(\mathbf{B}_0(t) + \sum_{j\neq i}\mathbf{B}_j(\mathbf{r}_{ij}, t)\right), \qquad (1)$$

where χ is the susceptibility of the particles with diameter σ, and μ_0 the vacuum permeability. The field induced by the j-th colloid at the position of the i-th colloid is given by

$$\mathbf{B}_j(\mathbf{r}_{ij}, t) = \frac{\mu_0}{4\pi}\frac{3(\mathbf{m}_j(t)\cdot\hat{\mathbf{r}}_{ij})\hat{\mathbf{r}}_{ij} - \mathbf{m}_j(t)}{r_{ij}^3}, \qquad (2)$$

A self-consistent procedure was adopted to solve the coupled equations (1) and (2) and compute the magnetic moments for every colloid in a given configuration. The magnetic force acting on the particle i is then obtained as a sum of dipole-dipole forces:

$$\mathbf{F}_i^M = \sum_j \mathbf{F}_{ji}^d(\mathbf{r}_{ij}) = \frac{3\mu_0}{4\pi r^4}\sum_j\Big((\mathbf{m}_i\cdot\hat{\mathbf{r}}_{ij})\,\mathbf{m}_j + \qquad (3)$$

$$+(\mathbf{m}_j\cdot\hat{\mathbf{r}}_{ij})\,\mathbf{m}_i + (\mathbf{m}_i\cdot\mathbf{m}_j)\,\hat{\mathbf{r}}_{ij} - 5\,(\mathbf{m}_i\cdot\hat{\mathbf{r}}_{ij})\,(\mathbf{m}_j\cdot\hat{\mathbf{r}}_{ij})\,\hat{\mathbf{r}}_{ij}\Big),$$

We assume a high frequency of the external field, in which case the magnetic moments of colloids are effectively time-averaged (the timescale on which particles translationally move is much larger than the timescale on which the field rotates). As Martin *et al.* [58] have shown this assumption simplifies the calculation of the magnetic forces: the time-averaged force is equal to the sum of the forces calculated with three static root-mean squared orthogonal field components $\mathbf{B}^A_{x,y,z}$, where $\mathbf{B}^A_k = \sqrt{\langle \mathbf{B}^2_{0,k}\rangle}$, i.e. $\mathbf{B}^A_x = \mathbf{B}^A_y = B_0\sin\theta/\sqrt{2}$ and $\mathbf{B}^A_z = B_0\cos\theta$. The total

Quantity	Reduced unit
Distance	σ
Field	B_0
Magnetic moment	$m_0 = B_0 \frac{4\pi\chi\sigma^3}{24\mu_0}$
Energy	$E_0 = m_0 B_0$
Force	E_0/σ
Temperature	$k_B T/E_0$
Mass	M_{colloid}
Time	$t_0 = \sqrt{\frac{M_{\text{colloid}}\sigma^2}{E_0}}$
Velocity	σ/t_0

TABLE I. Table of reduced units.

force on a particle,

$$\mathbf{F}_i = \mathbf{F}_i^{\mathrm{M}} + \mathbf{F}_i^{\mathrm{WCA}} + \mathbf{F}_i^{\mathrm{HD}} + \mathbf{F}_i^{\mathrm{F}} \ , \tag{4}$$

is composed of the interaction terms $\mathbf{F}_i^{\mathrm{M}} + \mathbf{F}_i^{\mathrm{WCA}}$, the hydrodynamic drag $\mathbf{F}_i^{\mathrm{HD}} = -\gamma \mathbf{v}_i = -3\pi\eta\sigma\mathbf{v}_i$ with η the fluid viscosity and $\mathbf{v}_i$ the particle velocity, and a random contribution to account for thermal fluctuations satisfying the following two conditions: i) $\langle \mathbf{F}_i^{\mathrm{F}} \rangle = 0$, and ii) $\langle \mathbf{F}_i^{\mathrm{F}}(t)\mathbf{F}_i^{\mathrm{F}}(t') \rangle = 6\, k_B T\, \xi\, \delta(t-t')$ with ξ a Gaussian distributed function with zero average and variance 1. To speed up simulations, we truncated the interaction potential at $7\,\sigma$ and we used a lower value for the fluid viscosity in order to achieve a faster relaxation: $\eta = \eta_{\text{water}}/47$. Since the system is planar, the correction due to the long-range nature of magnetic interactions is expected to be small. Recently, the same planar system of magnetic colloids was successfully modelled using only (short-ranged) patchy particles, which indicates that the long-range nature of magnetic interactions is not crucial in the case of 2D magnetic colloids [50].

To integrate the equations of motion we employed a recently developed scheme that is related to the velocity Verlet algorithm, and is appropriate for equilibrium and non-equilibrium Langevin dynamics simulations [60]. Throughout the work we use reduced units which are summarized in Table I. Based on previous work the magnetic susceptibility was chosen to be $\chi = 0.893$ [57], corresponding to micron size dynabeads superparamagnetic particles. Reduced temperature was set to $8.7 \cdot 10^{-5}$, which corresponds to an experimental system with colloids of diameter $\sigma \approx 1\,\mu$m and the field strength $B_0 \approx 10\,$mT. The systems consisted of 500 particles with a reduced number density $\rho^* = \rho\sigma^2 = 0.4$ confined to the xy-plane. First, equilibration runs were performed during which initially randomly dispersed colloids formed a matrix. Final configurations were taken as an initial state for shear simulations. The shear in x-direction was imposed through Lees-Edwards boundary conditions [61], which use a shear rate $\dot\gamma$ as an input parameter. For each shear rate between 90 and 600 independent runs were performed.

When a system was exposed to the shear flow in x-direction, the stress developed, which was computed as

$$\sigma_{xy} = \frac{1}{L^2}\Big\langle \sum_i \big[m_i(v_{i,x} - v_{s,x}(y))v_{i,y} + \sum_{j>i} r_{ij,x}F_{ij,y}\big]\Big\rangle, \tag{5}$$

where L is the length of simulation box and $v_{s,x}(y) = \dot\gamma(y - L/2)$. We found the kinetic contribution to be negligible.

III. RESULTS

A. Plastic flow and defect dynamics in crystals

Figure 2**A** presents the stress σ_{xy} as a function of the strain γ, for opening angle $\theta = 0°$. Different colors correspond to different shear rates $\dot\gamma$. The stress-strain relation has a typical fluid-like dependence: for small γ the stress increases linearly and at a strain $\gamma \approx 0.1$ it reaches a steady-state value. In our case the steady-state stress depends on the shear rate in a non-monotonic way. The corresponding velocity profiles $v_x(y)$ at two values of the strain, $\gamma = 0.1$ and $\gamma = 1$, are shown on Figure 2**B**. We notice a qualitative difference between the linear velocity profile at small shear rates and the formation of the shear bands at the boundaries $y \approx \pm L/2$ in case of $\dot\gamma = 4\cdot10^{-4}$. In the latter case, the timescale introduced by shearing is too short for a matrix to respond, therefore the effect is limited to the boundaries. In order to get a better insight into the response of the system to the external shear, we explored one trajectory ($\dot\gamma = 10^{-5}$) into more detail. The results are presented in Figure 3. The stress-strain

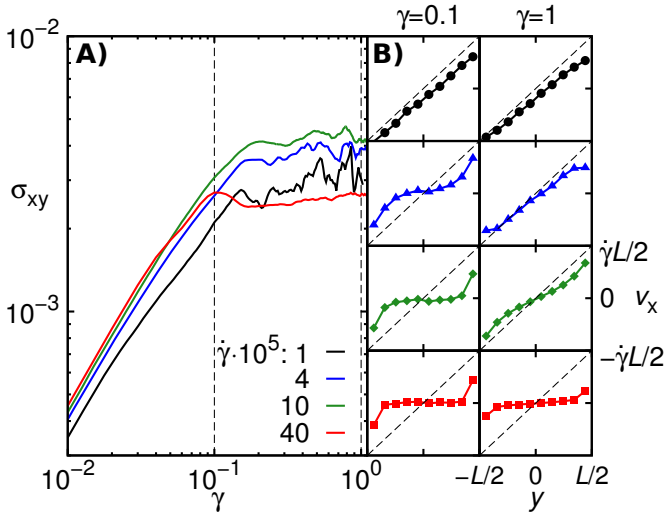

FIG. 2. **A)** The stress-strain relation, $\sigma_{xy}(\gamma)$, averaged over 600 trajectories at the opening angle $\theta = 0°$. **B)** The corresponding velocity profiles, $v_x(y)$, taken at strains $\gamma = 0.1$ and $\gamma = 1$ (as also indicated with dashed lines on **A**). The dashed lines on **B** represent linear velocity profiles of an ideal Newtonian fluid at corresponding conditions. Various colors correspond to different shear rates $\dot\gamma$.

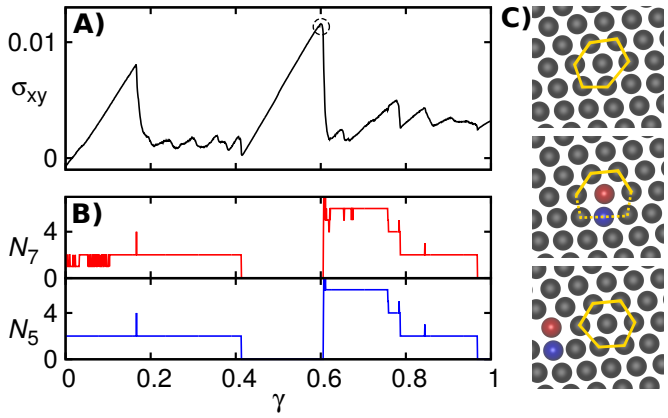

FIG. 3. **A)** The stress-strain relationship, $\sigma_{xy}(\gamma)$, for a single trajectory at the opening angle $\theta = 0°$ and shear rate $\dot{\gamma} = 10^{-5}$. **B)** Number of 5-fold (N_5; blue) and 7-fold disclinations (N_7; red) as a function of strain γ. **C)** A sequence of snapshots taken around the peak ($\gamma \approx 0.6$) designated by a dashed circle in **A)**. Time increases from top to bottom. Particles with 6 neighbours (as determined by Voronoi construction) are colored gray, with 5 blue, and those with 7 are red. Yellow lines are guides to the eye and represent nearest neighbours of the central particle.

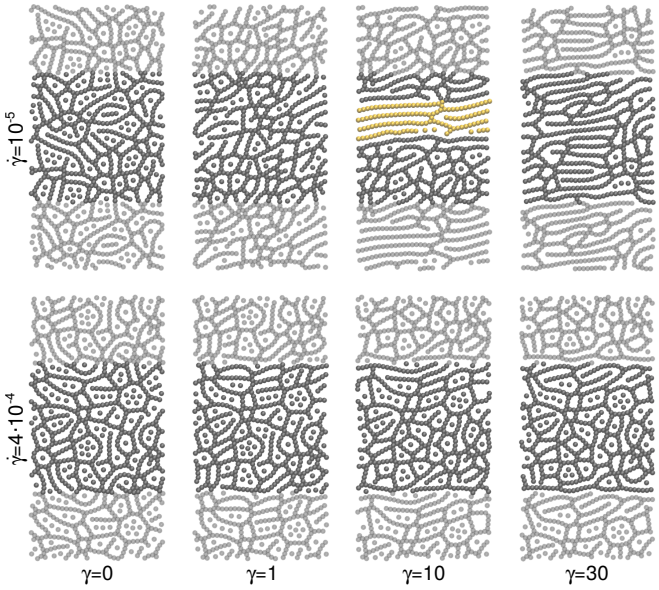

FIG. 4. Series of snapshots for the opening angle $\theta = 48°$ at the small (top row) and the large shear rate (bottom row) and at different strains γ (columns corresponding to the dashed lines in Figure 5**A**). Yellow color highlights the shear band and light gray color is used to depict the periodic images in y direction. The movies of the entire trajectories are shown in the Online SI.

curve (Figure 3**A**) exhibits characteristic irregularly occuring peaks of asymmetric shape with a constant slope that pertains up to the maximum stress followed by a sudden drop in σ_{xy}. Using the Voronoi construction we determined the coordination number of each particle and identified the defects. As expected, due to the strong repulsion between the colloids, the particles form a more or less perfect hexagonal lattice with occasional dislocation defects (pairs of 5- and 7-fold disclinations). On Figure 3**B** it can be seen that the number of dislocations (N_5=N_7) strongly correlates with the sudden drops in the stress σ_{xy}, which suggests that the mechanism of stress propagation is the formation, flow and annihilation of the defects. The structural rearrangements at the particle level are illustrated by three sequential snapshots in Figure 3**C**. The particles are colored according to their coordination number: gray (6), blue (5), and red (7). The nearest–neighbours cage is indicated by the solid yellow line. Upon applying shear, the initially hexagonal lattice deforms in the direction of the applied shear, the top snapshot shows such a deformation in the vicinity of a local temporal maximum of the stress σ_{xy} (the dashed circle in Figure 3**A**). Eventually, the system relaxes the stress through the formation of dislocations. The dislocations move until they are annihilated and the process starts again (see Online SI for trajectories).

B. Shear banding and gel deformation

At the opening angle $\theta = 48°$, in the absence of the applied shear, the system assembles into coexisting percolated network and free particles [50]. The free particles are repelled from the chains within the network, which stabilizes such structures. The structural changes following the application of shear are depicted by the snapshots in Figure 4 for the two extreme values of the shear rate (top row: $\dot{\gamma} = 10^{-5}$, bottom row: $\dot{\gamma} = 4 \cdot 10^{-4}$) and at given values of the strain (columns; the left column is the initial configuration prior to shearing). We observe almost no structural change at the larger shear rate, except for

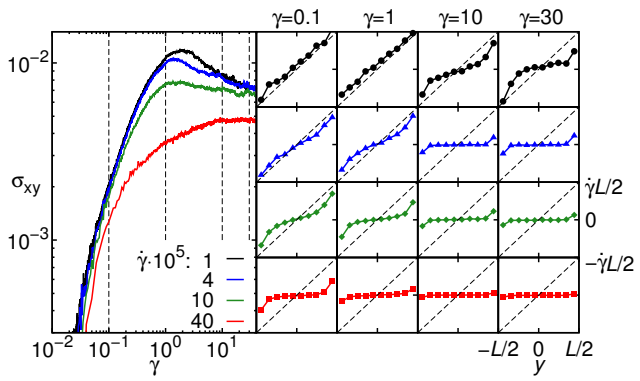

FIG. 5. **A)** The stress-strain relation, $\sigma_{xy}(\gamma)$, for the opening angle $\theta = 48°$. **B)** The corresponding velocity profiles, $v_x(y)$, taken at strains $\gamma = 0.1$, 1, 10 and 30 (as also indicated with dashed lines on **A**). Dashed lines represent linear velocity profiles of an ideal Newtonian fluid at corresponding conditions.

a narrow region at $y \approx \pm L/2$ where the chains of magnetic colloids are elongated in the direction of the shear. Analyzing the bond order parameter (see Online SI for details), we find that the number of particles forming two bonds grows at the expense of particles with three or more bonds, i.e. the branching points (Fig. S1 in Online SI). At the smaller shear rate, the behaviour is quite different: upon increasing the strain, the entire network gradually transforms by aligning the chains with the external shear direction, and by incorporating the free particles into the chains. At around $\gamma = 10$, transient shear bands emerge (designated by yellow color on Figure 4). Differently from the larger shear rate, where such bands only form at the boundaries, here they emerge at random positions within the system. With a further increase in the strain, the shear bands spread over the entire system ending up in a homogeneous steady state (the right most snapshot in the top row). This is a new steady state enabled by the applied shear. After switching off the shear, the stress only slightly decreases to a constant value that persists throughout the entire simulation with the order of 10^6 time steps (see Fig. S2 in Online SI). Since the time step is of the order of μs and the model viscosity is reduced, the simulation time corresponds to real times about two orders of magnitude larger than the typical time a colloid would diffuse its own diameter. The residual stress is therefore associated with a deformed configuration that is a metastable but long-lived state.

Stress-strain curves are plotted on Figure 5**A**. Different colors correspond to the same set of shear rates as on Figure 2**A**. While at the largest shear rate (red curve), the stress monotonically increases with the strain, the curves at smaller shear rates exhibit an initial linear regime, subsequent overshoot followed by a relaxation of the stress. Interestingly, the largest stress develops at the lowest shear rate (black line). An important point is that the maximum stress, $\sigma_{\max}$, is reached at the strain value of $\gamma \approx 1$, which is an order of magnitude larger than in the case of the opening angle $\theta = 0°$ as well as for glassy systems with a dense packing of particles (see, e.g., [21, 27]). Note that the maximum in the stress-strain relation can be seen as a yield point that marks the transition towards plastic flow. In densely packed system, $\sigma_{\max}$ occurs at a strain of the order of 0.1 which corresponds to the strain required to break the cage around a particle formed by its nearest neighbors [21]. The larger value of $\sigma_{\max}$ in our gel-like system indicates that it can be much more "elastically" deformed than a densely-packed glass before yielding occurs. A similar finding has also been found for other gel-like systems [44]. The corresponding velocity profiles $v_x(y)$ at strain values $\gamma = 0.1$, 1, 10 and 30 are plotted in Figure 5**B**. For the small shear rates, linear velocity profiles develop already at small strains, which subsequently flattens after the stress has reached the maximum ($\gamma \approx 1$). For the largest shear rate (red), the timescale introduced by shearing is very short, which localizes the deformation of the matrix to within narrow bands close to the boundaries $y \approx \pm L/2$, while leaving the bulk of the system unperturbed ($v_x = 0$).

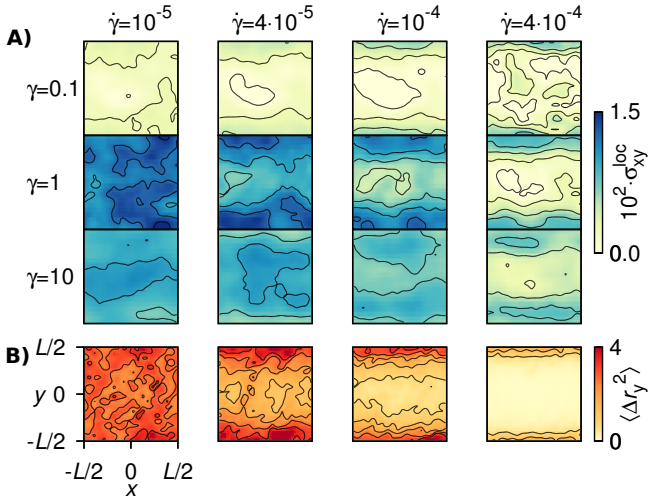

FIG. 6. **A)** Two-dimensional distribution of stress σ_{xy}^{loc} for the opening angle $\theta = 48°$ at strain $\gamma = 0.1$ (top row), $\gamma = 1$ (center) and $\gamma = 10$ (bottom row) for different shear rates $\dot{\gamma}$ (columns). **B)** Two-dimensional distribution of mean-squared displacement in y-direction $\langle \Delta r_y^2 \rangle$ at strain $\gamma = 1$ and different shear rates $\dot{\gamma}$ (columns).

In Figure 6**A**, the two-dimensional distribution of stress σ_{xy}^{loc} is shown at three different strain values and four different shear rates. For the smallest shear rate (left column), the stress is roughly uniformly distributed regardless of the strain. This is further illustrated by the non-affine deformations depicted by the heat map of the particle mean–squared displacement $\langle r_y^2 \rangle$ orthogonal to the shearing direction (Figure 6**B**). The uniform distribution and relatively large value of $\langle r_y^2 \rangle$ at the small shear rate allows an efficient transfer of stress from the boundaries to the bulk of the system. At larger shear rates, the particle bond orientation becomes highly anisotropic at the boundaries where the bonds are aligned with the external shear (see Online SI), the non-affine deformations are suppressed and localized (Figure 6**B**), which results in an inefficient transfer of the stress and its localization in the boundary regions (Figure 6**A**).

C. Shear-induced phase separation

Upon increasing the opening angle of the external field, the atractive part of the interparticle interaction starts to dominate the behaviour. At $\theta = 50°$ the unsheared structures are percolated networks that are metastable. Upon shearing, the colloids are pushed over the interaction barrier resulting in clustering and subsequent phase separation. Figure 7**A** presents the stress-strain relationship for this case. After an initial linear increase of σ_{xy} with γ, the maximum stress is achieved at $\gamma \approx 1$, followed by a steady decrease (i.e. the system does not reach a steady-state). The stress at large shear rate becomes

negative because at this conditions the system is unstable against phase separation. Accompanying structural changes for the small and large $\dot{\gamma}$ are illustrated with snapshots on Figure 7**B** (for examples of trajectories, see Online SI). The linear increase in the stress-strain curves is associated to the network deformation, while the onset of cluster formation is observed at $\gamma \approx 1$ – leading to the phase separation into a high-density and low-density regions at larger strain values. While for the small $\dot{\gamma}$ at $\gamma = 5$ the phase separation is not complete (there are still chains interconnecting dense clusters), it is almost complete at the largest shear rate.

The snapshots in Figure 7**B** suggest that the "final" state depends on the shear rate. We use the average coordination number, $\langle n \rangle$ (the number of particles that lie within a cutoff $r_{\rm cut} = 1.2\sigma$ of the central particle) as an order parameter to characterize the phases. It is shown as a function of the strain in Figure 8**A**. Indeed, we find that $\langle n \rangle$ grows with the shear rate, while the energy per particle E/N decreases with an increasing shear rate (see Figure 8**B**). Although it is difficult to claim that the system has reached its final state at the maximum accessible strain $\gamma = 20$, the data in Figure 7 – and the fact that the flow profile resembles the plug-flow – do indicate that a steady state is approached. The phase separation suggested by the snapshots in Figure 7 is confirmed with density profiles $\rho(y)$ in Figure 8**C**. Up to $\gamma = 1$ the number density profile is uniform, while at $\gamma = 10$ the system becomes heterogeneous with pronounced density fluctuations implying that the applied shear induces a phase transformation.

IV. SUMMARY AND CONCLUSIONS

We have studied the shear response of two-dimensional superparamagnetic colloids in a precessing magnetic field, whose structure changes from hexagonal crystal to an amorphous gel network upon varying the opening angle of the precessing field. At sufficiently low shear rates, the hexagonal crystal shows a transition towards plastic flow beyond a strain of the order of $\gamma = 0.1$, consisting of successive stress drops where the stress is released via the formation of dislocation defects. These findings are similar to those in previous studies of two-dimensional crystals, as obtained from colloid experiments [52, 53] and simulations [54, 55]. At the considered shear rates, the amorphous network structures do not evolve into a steady state; the common behavior is instead a plug-flow-like behavior at large strains. The stress-strain relations show a maximum around a strain $\gamma \approx 1.0$, marking the dynamic yield point of the networks. Particularly interesting is the shear response for the case $\theta = 48°$. Here, the system transforms into a stretched network structure via the formation of shear bands in an intermediate strain regime. The final stretched network is metastable also after the switch-off of the shear field. This indicates that shear can be used to generate metastable gels with an anisotropic structure. In the case of $\theta = 50°$, the network structure becomes unstable under shear and exhibits a phase separation into clusters with a hexagonal crystalline structure that are linked to each other by the remaining parts of the network.

As demonstrated in this work, the considered magnetic system can be used as a model for gels, ideally suited for elucidating the response of gels to an external mechanical loading. Moreover, it can be readily realized by colloidal experiments and analyzed via video microscopy. Its experimental realization under shear is a subject of forthcoming studies.

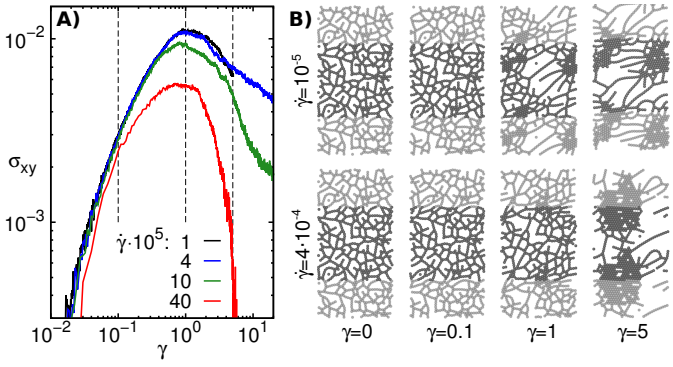

FIG. 7. **A)** The stress-strain relation, $\sigma_{\rm xy}(\gamma)$, for the opening angle $\theta = 50°$. **B)** The series of snapshots at small (top row) and large (bottom row) shear rate taken at different strains (the dashed lines on **A**). Periodic images in y–direction are depicted with the lighter gray color.

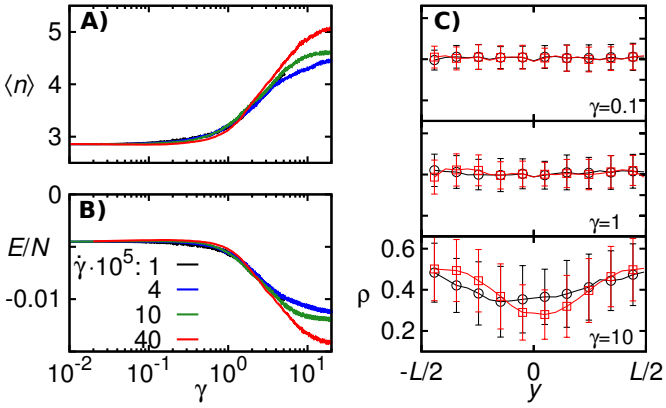

FIG. 8. **A)** The average coordination number $\langle n \rangle$ and **B)** the energy per particle E/N as a function of the strain γ. **C)** The density profile $\rho(y)$ for small (black circles) and large (red squares) shear rate at three different values of the strain.

V. ACKNOWLEDGEMENTS

This work was supported by the Fundamental Research Funds for the Central Universities of P. R. China

under the project buctrc201422, ERC Advanced Grant 227758 (COLSTRUCTION), and European ITN grant 234810 (COMPPLOIDS). J.H. acknowledges financial support by the Deutsche Forschungsgemeinschaft (DFG) in the framework of the priority programme SPP 1594 (Grant No. HO 2231/8-2) and T.M. by the Slovenian Research Agency (ARRS) funds through the Young Researchers Program.

[1] C. A. Schuh, T. C. Hufnagel, and U. Ramamurty, Acta Mater. **55**, 4067 (2007).
[2] L. Wondraczek, J. C. Mauro, J. Eckert, U. Kuhn, J. Horbach, J. Deubener, and T. Rouxel, Adv. Materials **23**, 4578 (2011).
[3] F. Varnik, L. Bocquet, and J.-L. Barrat, J. Chem. Phys. **120**, 2788 (2004).
[4] Y. Zhang, W. H. Wang, and A. L. Greer, Nature Mater. **5**, 857 (2006).
[5] A. L. Greer, Y. Q. Cheng, and E. Ma, Mater. Sci. Eng. R **74**, 71 (2013).
[6] N. P. Bailey, J. Schiotz, and K. W. Jacobsen, Phys. Rev. B **73**, 064108 (2006).
[7] J. Bokeloh, S. V. Divinski, G. Reglitz, and G. Wilde, Phys. Rev. Lett. **107**, 235503 (2011).
[8] H. Rösner, M. Peterlechner, C. Kübel, V. Schmidt, and G. Wilde, Ultramicroscopy **142**, 1 (2014).
[9] V. Schmidt, H. Rösner, M. Peterlechner, G. Wilde, and P. M. Voyles, Phys. Rev. Lett. **115**, 035501 (2015).
[10] D. Rodney, A. Tanguy, and D. Vandembroucq, Modelling Simul. Mater. Sci. Eng. **19**, 083001 (2011).
[11] M. L. Falk, and C. E. Maloney, Eur. Phys. J. B **75**, 405 (2010).
[12] Y. Shi and M. L. Falk, Phys. Rev. B **73**, 214201 (2006).
[13] S. Karmakar, E. Lerner, and I. Procaccia, Phys. Rev. E **82**, 055103(R) (2010).
[14] J. Chattoraj, C. Caroli, and A. Lemaitre, Phys. Rev. Lett. **105**, 266001 (2010).
[15] V. Chikkadi, G. Wegdam, D. Bonn, B. Nienhuis, and P. Schall, Phys. Rev. Lett. **107**, 198303 (2011).
[16] R. Dasgupta, H. G. E. Hentschel, and I. Procaccia, Phys. Rev. Lett. **109** 255502 (2012).
[17] R. Besseling, L. Isa, P. Ballesta, G. Petekidis, M. E. Cates, and W. C. K. Poon, Phys. Rev. Lett. **105**, 268301 (2010).
[18] K. Martens, L. Bocquet, and J.-L. Barrat, Soft Matter **8**, 4197 (2012).
[19] S. M. Fielding, Rep. Prog. Phys. **77**, 102601 (2014).
[20] E. Irani, P. Chaudhuri, and C. Heussinger, Phys. Rev. Lett. **112**, 188303 (2014).
[21] J. Zausch, J. Horbach, M. Laurati, S. U. Egelhaaf, J. M. Brader, T. Voigtmann, and M. Fuchs, J. Phys.: Condens. Matter **20**, 404120 (2008).
[22] J. Zausch and J. Horbach, EPL **88**, 60001 (2009).
[23] P. Chaudhuri and J. Horbach, Phys. Rev. E **88**, 040301(R) (2013).
[24] Chaudhuri, P. and Horbach, J. Phys. Rev. E **90**, 040301(R) (2014).
[25] M. Ballauff, J. M. Brader, S. U. Egelhaaf, M. Fuchs, J. Horbach, N. Koumakis, M. Krüger, M. Laurati, K. J. Mutch, M. Siebenbürger, T. Voigtmann, and J. Zausch, Phys. Rev. Lett. **110**, 215701 (2013).
[26] Sentjabrskaja, T., Chaudhuri, P., Hermes, M., Poon, W. C. K., Horbach, J., Egelhaaf, S. U., and Laurati, M. Sci. Rep. **5**, 11884 (2015).
[27] G. P. Shrivastav, P. Chaudhuri, and J. Horbach, preprint arXiv:1506.03049.
[28] I. Binkowski, G. P. Shrivastav, J. Horbach, S. V. Divinski, and G. Wilde, unpublished.
[29] N. Kern and D. Frenkel, J. Chem. Phys. **118**, 9882 (2003).
[30] M. Laurati, G. Petekidis, N. Koumakis, F. Cardinaux, A. B. Schofield, J. M. Brader, M. Fuchs, and S. U. Egelhaaf, J. Chem. Phys. **130**, 134907 (2009).
[31] F. Sciortino and E. Zaccarelli, Curr. Op. Solid State Mater. Sci. **15**, 246 (2011).
[32] E. Bianchi, R. Blaak, and C. N. Likos, Phys. Chem. Chem. Phys. **13**, 6397 (2011).
[33] S. Romer, H. Bissig, P. Schurtenberger, and F. Scheffold, EPL **108**, 48006 (2014).
[34] S. T. Milner, Phys. Rev. E **48**, 3674 (1993).
[35] C. Storm, J. J. Pastore, F. C. MacKintosh, T. C. Lubensky, and P. A. Janmey, Nature **435**, 191 (2005).
[36] P. A. Janmey, M. E. McCormick, S. Rammensee, J. L. Leight, P. C. Georges, and F. C. MacKintosh, Nature Mater. **6**, 48 (2007).
[37] O. Lieleg, M. M. A. E. Claessens, C. Heussinger, E. Frey, and A. R. Bausch, Phys. Rev. Lett. **99**, 088102 (2007).
[38] P. Cordier, F. Tournilhac, C. Soulie-Ziakovic, and L. Leibler, Nature **451**, 977 (2008).
[39] B. Mantisi, A. Tanguy, G. Kermouche, and E. Barthel, Eur. Phys. J. B **85**, 304 (2012).
[40] N. S. Shcheblanov, B. Mantisi, P. Umari, and A. Tanguy, J. Non-Cryst. Solids **428**, 6 (2015).
[41] T. Divoux, D. Tamarii, C. Barentin, and S. Manneville, Phys. Rev. Lett. **104**, 208301 (2010).
[42] A. Kurokawa, V. Vidal, K. Kurita, T. Divoux, and S. Manneville, Soft Matter **11**, 9026 (2015).
[43] J. Colombo, A. Widmer-Cooper, and E. Del Gado, Phys. Rev. Lett. **110**, 198301 (2013).
[44] J. Colombo and E. Del Gado, J.Rheol. **58**, 1089 (2014).
[45] A. Mohraz and M. J. Solomon, J. Rheol. **49**, 657 (2005).
[46] V. Schmitt, C. M. Marques, and F. Lequeux, Phys. Rev. E **52**, 4009 (1995).
[47] H. Tanaka and T. Araki, EPL **79**, 58003 (2007).
[48] A. Onuki, J. Phys. II **2**, 45 (1992).
[49] A. Onuki, Adv. Polymer Sci. **109**, 63 (1993).
[50] K. Müller, N. Osterman, D. Babić, C. N. Likos, J. Dobnikar, and A. Nikoubashman, Langmuir **30**, 5088 (2014).
[51] J. P. Poirier, *Creep of Crystals* (Cambridge Univ. Press, Cambridge, 1985).
[52] C. Eisenmann, U. Gasser, P. Keim, G. Maret, and H. H. von Grünberg, Phys. Rev. Lett. **95**, 185502 (2005).
[53] W. Lechner, D. Polster, D. Maret, P. Keim, and C. Dellago, Phys. Rev. E **88**, 060402(R) (2013).
[54] T. Horn and H. Löwen, J. Chem. Phys. **141**, 224505 (2014).
[55] S. Ganguly, S. Sengupta, and P. Sollich, Soft Matter **11**, 4517 (2015).

[56] J. D. Weeks, D. Chandler, and H. C. Andersen, J. Chem. Phys. **54**, 5237 (1971).
[57] N. Osterman, I. Poberaj, J. Dobnikar, D. Frenkel, P. Ziherl, and D. Babić, Phys. Rev. Lett. **103**, 228301 (2009).
[58] J. E. Martin, R. A. Anderson, and R. L. Williamson, J. Chem. Phys. **118**, 1557 (2003).
[59] I. M. Kulic and M. L. Kulic, Phys. Rev. Lett. **111**, 198301 (2013).
[60] D. A. Sivak, J. D. Chodera, and G. E. Crooks, J. Phys. Chem. B **118**, 6466 (2014)
[61] A. W. Lees and S. F. Edwards, J. Phys. C **5**, 1921 (1972).